27. E. Canales, E. J. Corey, *J. Am. Chem. Soc.* **129**, 12686–12687 (2007).
28. P. Karrer, F. Canal, K. Zohner, R. Widmer, *Helv. Chim. Acta* **11**, 1062–1084 (1928).
29. M. Hajri, C. Blondelle, A. Martinez, J.-L. Vasse, J. Szymoniak, *Tetrahedron Lett.* **54**, 1029–1031 (2013).
30. G. Adamson, A. L. J. Beckwith, M. Kaufmann, A. C. Willis, *J. Chem. Soc. Chem. Commun.* **1995**, 1783–1784 (1995).
31. D. J. Robins, D. S. Rycroft, *Magn. Reson. Chem.* **30**, 1125–1127 (1992).
32. D. Gray, T. Gallagher, *Angew. Chem. Int. Ed.* **45**, 2419–2423 (2006).

Acknowledgments: This work was supported by the Deutsche Forschungsgemeinschaft (Graduiertenkolleg GRK 1626 Chemical Photocatalysis) and by the Fonds der Chemischen Industrie (scholarship to R.B.). We thank O. Ackermann for help in conducting HPLC analyses.

Supplementary Materials
www.sciencemag.org/content/342/6160/840/suppl/DC1
Supplementary Text
Figs. S1 to S8
NMR Spectra
HPLC Spectra
References (*33*–*42*)

16 August 2013; accepted 16 October 2013
10.1126/science.1244809

Abrupt Shifts in Horn of Africa Hydroclimate Since the Last Glacial Maximum

Jessica E. Tierney[1]* and Peter B. deMenocal[2]

The timing and abruptness of the initiation and termination of the Early Holocene African Humid Period are subjects of ongoing debate, with direct consequences for our understanding of abrupt climate change, paleoenvironments, and early human cultural development. Here, we provide proxy evidence from the Horn of Africa region that documents abrupt transitions into and out of the African Humid Period in northeast Africa. Similar and generally synchronous abrupt transitions at other East African sites suggest that rapid shifts in hydroclimate are a regionally coherent feature. Our analysis suggests that the termination of the African Humid Period in the Horn of Africa occurred within centuries, underscoring the nonlinearity of the region's hydroclimate.

During the Early Holocene epoch between roughly 11 to 5 thousand years ago (ka), the presently hyperarid Saharan desert was dotted with large and small lakes, savannah grasslands, and in some regions, humid tropical forests and shrubs (*1*, *2*). This "African Humid Period" (AHP) was a unique hydrological regime and has been a focal point of African paleoclimate studies, both for its climatological implications (*3*, *4*) and its influence on the emergence of pharaonic civilization along the Nile (*5*, *6*). The fundamental cause of the AHP—dramatic increases in summer precipitation triggered by orbital forcing of African monsoonal climate and amplified by oceanic and terrestrial feedbacks—is well understood (*7*, *8*). However, the abruptness with which the AHP began and, most particularly, ended is still debated. Dust proxy data from the west coast of Africa indicate a rapid, century-scale termination of the AHP near 5 ka (*9*). In contrast, isotopic proxies from central Africa (*10*, *11*) and pollen and sedimentological data from a lake in the eastern Sahara (*12*, *13*) suggest a more gradual reduction in rainfall during the mid-Holocene tracking the orbital decline in boreal summer insolation. The discrepancy remains unresolved. Previous studies have attributed the difference in climate response to differing proxy sensitivities; for example, dust may respond nonlinearly to a gradual drying of the Sahara (*14*), and conversely, pollen data may be smoothed because of mixed contributions from distal terrains (*2*). Alternatively, there may be regional heterogeneity in both the timing and duration of the AHP termination, reflecting the variable sensitivity of different regions to certain feedback mechanisms (in particular, vegetation feedbacks) (*3*, *4*, *6*, *15*, *16*).

East Africa and the Arabian Peninsula also experienced humid conditions during the Early Holocene (*17*, *18*). Speleothem $\delta^{18}O$ data from southern Oman (Qunf Cave) and dust strontium isotopes off of Somalia suggest a gradual attenuation of humid conditions during the Holocene, much like the eastern Saharan pollen data (*19*, *20*). These observations have led to the suggestion that the eastern Sahara and northeast Africa experienced a gradual end to the AHP (*3*, *4*, *12*, *15*, *21*) and that abrupt responses were therefore limited to the western Sahara.

We revisited the timing and abruptness of transitions into and out of the AHP in northeast Africa using a new record of hydroclimate from a key, yet previously understudied, region: the Horn of Africa. This record is derived from a marine core (P178-15P) located in the Gulf of Aden (Fig. 1). The Gulf of Aden receives substantial amounts of terrestrial material during the summer monsoon season, when prevailing southwesterly winds transport dust from the Horn (Fig. 1 and fig. S1). Therefore, the terrestrial components (including organic matter) in the sediments predominantly reflect conditions in the Horn and Afar regions (supplementary materials). Twenty radiocarbon dates constrain the chronology of P178-15P and indicate an average sedimentation rate of 32 cm per thousand years (supplementary materials).

We used the hydrogen isotopic composition of leaf waxes (δD_{wax}) as a proxy for aridity and, more generally speaking, hydroclimate, including precipitation/evaporation balance and changes in regional convection. δD_{wax} has been widely used in African paleoclimate and is an effective indicator of changes in the isotopic composition of precipitation (δD_P) and aridity, with enriched isotopic values corresponding to drier conditions and depleted values to wetter conditions (*10*, *22*). More generally, tropical water isotopes are good tracers of large-scale changes in atmospheric circulation (*18*, *23*) and therefore reflect regional, rather than local, shifts in the hydrological cycle. Because Congo basin moisture is effectively blocked by the Ethiopian highlands and the Horn of Africa receives the majority of its rainfall from the Indian Ocean (*24*), we interpret the δD_{wax} values to primarily represent changes in western Indian Ocean hydroclimate.

The δD_{wax} record from the Gulf of Aden indicates that Horn of Africa hydroclimate has changed dramatically during the past 40,000 years (Fig. 2). After the arid conditions of the Last Glacial Maximum (LGM) (26 to 19 ka), the Horn region experienced a severe dry period coincident with the North Atlantic cooling event, Heinrich Event 1 (H1) (Fig. 2), which is consistent with previous proxy (*25*) and model (*23*) evidence

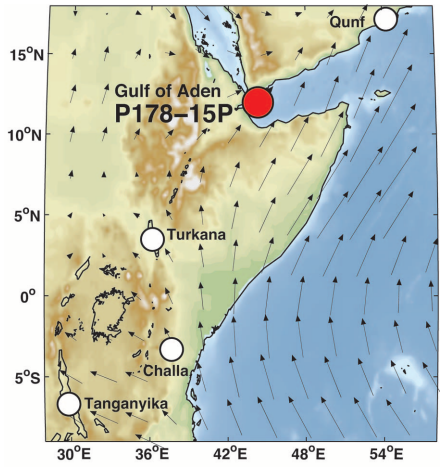

Fig. 1. A map of East Africa. The map includes topography, wind climatology for June-July-August (JJA) (*46*), the location of the study site (Gulf of Aden P178-15P; 11° 57.3′ N, 44° 18′ E, 869 m water depth), and other sites mentioned in the text.

[1]Woods Hole Oceanographic Institution, 266 Woods Hole Road, Woods Hole, MA 02540, USA. [2]Lamont Doherty Earth Observatory, Palisades, NY 10964, USA.

*Corresponding author. E-mail: tierney@whoi.edu

from the Afro-Asian monsoon domain. After H1, there was a rapid transition to intermediate conditions coincident with the Bölling-Allerød (B/A) period and then a reversal into dry conditions during the Younger Dryas (YD), another North Atlantic cold event (Fig. 2). Upon the termination of the YD, the Horn of Africa rapidly moved into the most humid conditions of the past 40,000 years, coincident with the AHP (Fig. 2). These conditions persisted until ~5 ka.

The δD_{wax} record from the Gulf of Aden is dominated by abrupt transitions that occur more rapidly than would be predicted from orbital forcing alone (Fig. 3). Two other δD_{wax} records from East Africa—from Lake Tanganyika (*22*) and Lake Challa (*26*)—show similar and generally coeval abrupt transitions at the end of H1, the YD, and the AHP, even though these sites sit ~2000 km to the south of the Gulf of Aden (Figs. 1 and 3). The overall similarity between the three records attests to the ability of water isotope proxies, specifically δD_{wax}, to record large-scale hydroclimatic patterns in tropical Africa.

The perceived timing and abruptness of the transitions in each δD_{wax} record is subject to dating uncertainties as well as sedimentary properties. Therefore, we used a Monte Carlo method (*27*) to create empirical probability distributions for the midpoint and duration of each identified transition and more clearly assess the duration and synchronicity of these key climate transitions (supplementary materials). We used these distributions to assess the timing of the transitions in a statistical fashion by applying a *T* test for contemporaneity (*28*) to test against the null hypothesis that the transitions are synchronous between two sites, or a χ^2 test to test against the null hypothesis that the transitions at all three sites derive from the same mean and are therefore likely synchronous. In both cases, we accepted the null hypothesis if $P > 0.05$.

Several findings emerged from this analysis. First, we found that the termination of H1 and the YD are not likely synchronous at all sites. All age model iterations indicate an older timing for the H1–B/A transition at Lake Tanganyika than at the Gulf of Aden site [Lake Challa does not have a detectable H1 termination (supplementary materials)]. The median date of the transition in the Gulf of Aden record [14,680 years before the present (B.P.)] is close to the generally accepted timing of 14,700 years B.P. (*29*), whereas the transition at Lake Tanganyika occurs nearly 1000 years earlier (median = 15,760 years B.P.). For the Challa and Tanganyika sites, the termination of the YD is likely synchronous (*t* test, $P = 0.99$) and the timing (median of both = 11,600 years B.P.) is in good agreement with the transition (11,570 years B.P.) dated by tree-ring chronologies (*30*), but the transition in the Gulf of Aden record occurs later in all iterations (median = 10,850 years B.P.).

The observed offsets in the Tanganyika and Aden δD_{wax} data across the H1 and YD terminations, respectively, could reflect meaningful local climatic deviations; however, because these millennial-scale events are remotely forced by North Atlantic processes, it seems more likely that they reflect unconstrained changes in site radiocarbon (^{14}C) reservoirs. Lake Tanganyika has a substantial ^{14}C reservoir today (~1000 years) owing to its meromixis (*22*), and although the evolution of this reservoir is constrained by paired bulk organic matter and terrestrial plant macrofossil dates from the LGM to present (*22*), no data are available for H1, during which time the lake was stratified (*31*). Likewise, we lack sufficient information to constrain how the Gulf of Aden ^{14}C reservoir has evolved through time. Although our site sits outside of the upwelling zone, it is still likely that the regional radiocarbon reservoir was modulated by the intensity of Arabian Sea upwelling, especially during the deglaciation, when large changes

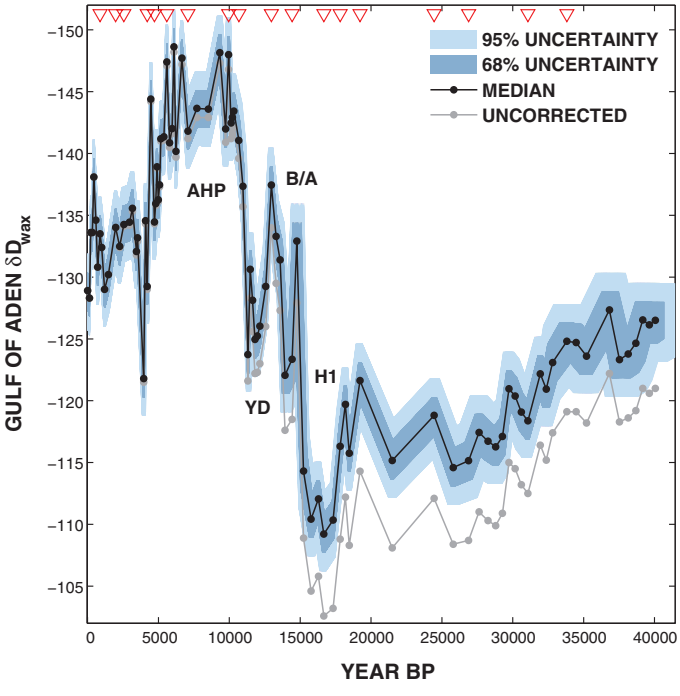

Fig. 2. δD_{wax} data from Gulf of Aden core P178-15P. δD_{wax} data is in per mil versus Vienna standard mean ocean water (VSMOW). Black line denotes median values, with the effect of changing ice volume on the isotopic values removed to isolate the regional hydroclimatic component (supplementary materials). Gray line shows the δD_{wax} data uncorrected for ice volume changes. Shadings indicate empirical 68 and 95% uncertainty bounds (including both analytical- and time-uncertainty) calculated via a Monte Carlo method (*27*). Red triangles denote the stratigraphic locations of radiocarbon dates.

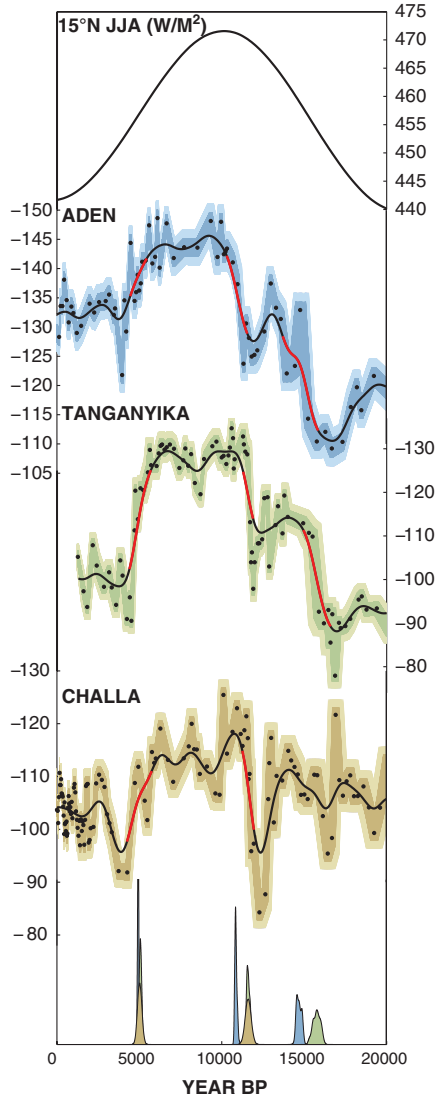

Fig. 3. JJA insolation at 15°N, δD_{wax} data from three sites in East Africa, and the timing of their abrupt transitions. JJA insolation is in watts per square meter, and δD_{wax} data is in per mil versus VSMOW. The effect of changing ice volume on the isotopic values has been removed to isolate the regional hydroclimatic component (supplementary materials). Black markers denote median values, and shadings indicate empirical 68 and 95% uncertainty bounds (including both analytical- and time-uncertainty) calculated via a Monte Carlo method (*27*). Black line indicates the 2000-year Gaussian smoothed time series for each site, with the identified transitions highlighted in red. Probability distributions (bottom) represent the timing of each highlighted transition given the dating uncertainties. Lake Challa δD_{wax} does not indicate a large drying associated with H1 and therefore lacks a H1–B/A transition (supplementary materials).

are known to have occurred and, at least in the eastern Arabian Sea, shifted the ^{14}C reservoir (*32*).

In contrast to the deglacial transitions, our analysis suggests that the termination of the AHP is likely synchronous between all three sites (χ^2 test, $P = 0.25$). Because the mid-Holocene is less likely to be affected by unknown uncertainties in the ^{14}C reservoir (*22*, *32*), we have more confidence that the inferred synchronicity is meaningful. Using Gaussian error reduction, the average timing of the AHP termination from these three East African sites is 4960 ± 70 years B.P. (2σ). This is similar to the revised AHP termination estimate from west Africa of 4900 ± 400 years B.P. (2σ) and is likely synchronous (*t* test, $P = 0.77$).

The observed durations of the identified transitions vary from centuries to millennia (Fig. 4); however, sedimentary factors (sedimentation rates and bioturbation) as well as the sampling rate of the proxy influence how the duration is expressed and attenuated in the time series. As evidence of this, we observed a strong relationship between the duration of the transition and proxy sampling interval (ΔT) [correlation coefficinet (r) = 0.95, $P = 0.0005$] (fig. S2). Normalizing the duration distributions by this sedimentation effect, we arrived at "theoretical" durations representing the most probable duration given a hypothetical infinite sampling rate (Fig. 4). We found that the calculated theoretical durations are short—occurring within centuries—and broadly similar between sites (Fig. 4). The theoretical duration of the termination of the AHP in our Gulf of Aden record ranges from 280 to 490 years. This duration is in accord with a recent analysis of lake level changes in Lake Turkana in northern Kenya: Detailed radiocarbon dating of exposed paleoshoreline horizons revealed that the water level in Lake Turkana dropped permanently by ~50 m within a few centuries at 5270 ± 300 years B.P. (also synchronous with our analyzed timing; *t* test, $P = 0.46$) (*33*). Taken together with our new data from the Gulf of Aden, this suggests that the termination of the AHP was abrupt across a relatively large sector of northeast Africa.

We recognize, however, that there is heterogeneity in terms of the timing and abruptness of the AHP termination across Africa according to the currently available proxy data. Although at low-resolution ($n = 29$ samples; mean ΔT = 470 years), a δD_{wax} record from Lake Victoria has been interpreted as reflecting a gradual termination of the AHP (*34*). Farther to the west, a δD_{wax} record that integrates the Congo drainage basin also shows a gradual termination (*10*), as does a record of the oxygen isotopic composition of seawater from the Gulf of Guinea (*11*). Likewise, to the north of our study site, $\delta^{18}O$ data measured on a Oman stalagmite from Qunf Cave (Fig. 1) suggests a gradual reduction in precipitation across the Arabian Peninsula (*19*). Collectively, these data suggest that abrupt behavior is not a universal feature across Africa and may be restricted to the western Sahara and East Africa.

If this is so, then the feedback mechanisms leading to the observed abrupt shifts may be relatively specific to these regions. In the Sahara and Sahel region, the nonlinear change in rainfall associated with the termination of the AHP likely involves vegetation feedbacks, which enhance the orbitally driven response by changing surface albedo and soil moisture (*35*, *36*). In contrast, vegetation feedbacks are not likely to have occurred within the humid central African zone, where proxy data suggest that vegetation has not shifted substantially (*10*). This may explain the lack of abrupt response in that region. Vegetation feedbacks are also hypothesized to be weaker in the eastern Saharan region because of regional differences in vegetation and soil moisture (*3*, *4*, *15*). In the extreme case, the Arabian Peninsula may not have acquired enough vegetation in the Early Holocene to promote a feedback in spite of more pluvial conditions; limited pollen data suggest a predominance of steppe and grassland but no development of shrubland or dry woodland (*1*, *37*). It is not clear whether vegetation feedbacks universally contributed to the abrupt shifts in East African hydroclimate. Carbon isotopes measured on the same leaf waxes at the sites analyzed here suggest that a vegetation feedback is plausible at Lake Tanganyika, which experienced a dramatic shift from a mixed humid woodland to a more open shrubland (fig. S3). However, there was relatively little shift in the vegetation near Lake Challa and in the Horn of Africa (fig. S3), suggesting that, as with the Arabian Peninsula, a vegetation-driven feedback is unlikely in arid East Africa.

Alternatively, we hypothesize that nonlinear behavior in East African rainfall, including the termination of the AHP, reflects convection feedbacks associated with Indian Ocean sea-surface temperatures (SSTs). This mechanism may explain the difference between the northeast African region and southern Oman. SSTs in the western Indian Ocean hover near the lower bound of the threshold for deep convection (26° to 28°C), and their relationship with deep convection is nonlinear (*38*). Therefore, very small changes in western Indian Ocean SSTs—such as those that occur during Indian Ocean Dipole or El Niño events, as well as oscillations on the multidecadal time scale—can alter the Walker Circulation in the Indian Ocean and induce anomalous deep convection and heavy rainfall in East Africa (*39*, *40*). Rainfall over the southern Arabian Peninsula, although susceptible to such variability (*41*), primarily falls from July through August in association with the Indian summer monsoon, and the influence of the latter likely dominates on orbital time scales (*19*, *21*). Therefore, whereas the gradual trend in the Qunf Cave speleothem record represents the direct response of Arabian hydroclimate to the orbitally driven waning of the boreal summer Indian monsoon, the abrupt shift in East Africa conceivably reflects a convective feedback with a different seasonal dimension. Model simulations suggest that during the Early Holocene, the northward migration of the summer monsoon winds in response to orbital forcing decreased latent heat flux out of the western Indian Ocean, leading to warmer SSTs during the following September-November ("short") rainy season, a reduced east-west SST gradient, and enhanced convection and rainfall over East Africa (*18*, *42*). As the winds migrated south during the Holocene in response to orbital forcing, a critical SST threshold may have been crossed, causing an abrupt cessation of deep convection during the short rainy season and regional aridity. Existing proxy data from the Arabian Sea indicate that Early Holocene SSTs were similar to, or perhaps slightly warmer than, present-day SSTs (*43*, *44*). Meanwhile, eastern Indian Ocean temperatures were slightly cooler (*45*), suggesting a reduced east-west temperature gradient that may have facilitated enhanced convection over East Africa, which is in agreement with the modeling results. It is unclear, however, whether these proxy data are reflecting a change in SSTs during a particular season.

Although further research is needed to investigate the role of Indian Ocean SSTs, the δD_{wax} data presented here suggest that the hydroclimate

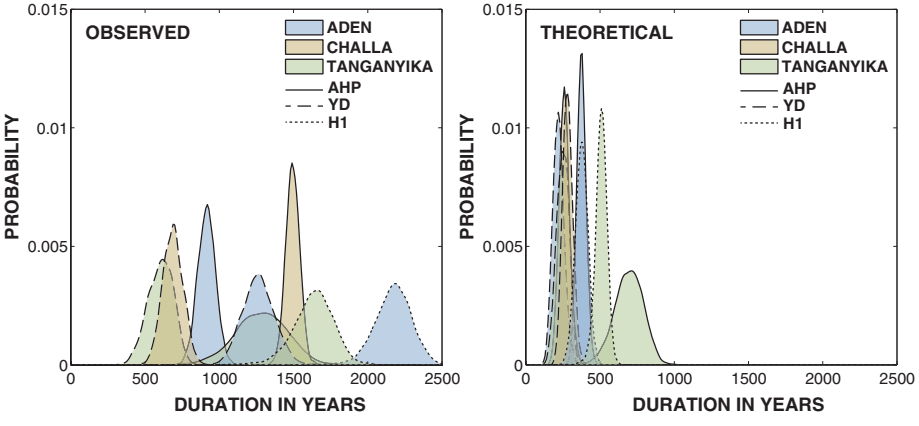

Fig. 4. Observed and theoretical probability distributions. Probability distributions are for the duration of the H1, YD, and AHP terminations at each East African site, corrected for the sampling interval effect (supplementary materials).

of East Africa can rapidly shift from dry and wet conditions. More generally, the Gulf of Aden δD_{wax} record provides a new benchmark of hydroclimatic history for the understudied Horn of Africa region. This study revises our understanding of Holocene climate change in northeast Africa, providing firm evidence that the abrupt termination of the AHP is not limited to the western Sahara. Although the forcings driving the abrupt shifts seen in the paleorecord since the LGM are large and not directly analogous to climate changes experienced today, the possibility of rapid changes in rainfall on human-relevant time scales (centuries) deserves further attention. Paleoclimate data from the past millennium suggest that easternmost Africa was much wetter than present only 300 years ago (*40*), attesting to the dynamic nature of the hydrological cycle in this region. Identifying the mechanisms driving these dramatic and rapid shifts in East African hydroclimate would greatly improve our understanding of the region's climatology, as well as future predictions of food and water security.

References and Notes

1. D. Jolly *et al.*, *J. Biogeogr.* **25**, 1007–1027 (1998).
2. A.-M. Lézine, C. Hély, C. Grenier, P. Braconnot, G. Krinner, *Quat. Sci. Rev.* **30**, 3001–3012 (2011).
3. V. Brovkin, M. Claussen, V. Petoukhov, A. Ganopolski, *J. Geophys. Res.* **103**, 31613 (1998).
4. M. Claussen *et al.*, *Geophys. Res. Lett.* **26**, 2037–2040 (1999).
5. P. Hoelzmann, B. Keding, H. Berke, S. Kröpelin, H.-J. Kruse, *Palaeogeogr. Palaeoclimatol. Palaeoecol.* **169**, 193–217 (2001).
6. R. Kuper, S. Kröpelin, *Science* **313**, 803–807 (2006).
7. J. E. Kutzbach, B. L. Otto-Bliesner, *J. Atmos. Sci.* **39**, 1177–1188 (1982).
8. M. Claussen, V. Gayler, *Global Ecol. Biogeo. Lett.* **6**, 369–377 (1997).
9. P. B. deMenocal *et al.*, *Quat. Sci. Rev.* **19**, 347–361 (2000).
10. E. Schefuß, S. Schouten, R. R. Schneider, *Nature* **437**, 1003–1006 (2005).
11. S. Weldeab, D. W. Lea, R. R. Schneider, N. Andersen, *Science* **316**, 1303–1307 (2007).
12. S. Kröpelin *et al.*, *Science* **320**, 765–768 (2008).
13. P. Francus *et al.*, *Sedimentology* **60**, 911–934 (2013).
14. J. A. Holmes, *Science* **320**, 752–753 (2008).
15. V. Brovkin, M. Claussen, *Science* **322**, 1326b (2008).
16. S. Bathiany, M. Claussen, K. Fraedrich, *Clim. Dyn.* **38**, 1775–1790 (2012).
17. F. A. Street-Perrott, D. S. Marchand, N. Roberts, S. P. Harrison, *U.S. Department of Energy Technical Report* 46 (U.S. Department of Energy Washington, DC, 1989).
18. J. E. Tierney, S. C. Lewis, B. I. Cook, A. N. LeGrande, G. A. Schmidt, *Earth Planet. Sci. Lett.* **307**, 103–112 (2011).
19. D. Fleitmann *et al.*, *Science* **300**, 1737–1739 (2003).
20. S. Jung, G. Davies, G. Ganssen, D. Kroon, *Earth Planet. Sci. Lett.* **221**, 27–37 (2004).
21. D. Fleitmann *et al.*, *Quat. Sci. Rev.* **26**, 170–188 (2007).
22. J. E. Tierney *et al.*, *Science* **322**, 252–255 (2008).
23. F. Pausata, D. Battisti, K. Nisancioglu, C. Bitz, *Nat. Geosci.* **4**, 474–480 (2011).
24. J. Slingo, H. Spencer, B. Hoskins, P. Berrisford, E. Black, *Philos. Trans. A Math. Phys. Eng. Sci.* **363**, 25–42 (2005).
25. J. C. Stager, D. B. Ryves, B. M. Chase, F. S. Pausata, *Science* **331**, 1299–1302 (2011).
26. J. E. Tierney, J. M. Russell, J. S. Sinninghe Damsté, Y. Huang, D. Verschuren, *Quat. Sci. Rev.* **30**, 798–807 (2011).
27. K. J. Anchukaitis, J. E. Tierney, *Clim. Dyn.* **41**, 1291–1306 (2013).
28. A. Long, B. Rippeteau, *Am. Antiq.* **39**, 205 (1974).
29. K. A. Hughen, T. I. Eglinton, L. Xu, M. C. Makou, *Science* **304**, 1955–1959 (2004).
30. M. Friedrich, B. Kromer, M. Spurk, J. Hofmann, K. Felix Kaiser, *Quat. Int.* **61**, 27–39 (1999).
31. J. E. Tierney, J. M. Russell, *Geophys. Res. Lett.* **34**, L15709 (2007).
32. M. Staubwasser, F. Sirocko, P. M. Grootes, H. Erlenkeuser, *Paleoceanography* **17**, 15-1–15-2 (2002).
33. Y. Garcin, D. Melnick, M. R. Strecker, D. Olago, J.-J. Tiercelin, *Earth Planet. Sci. Lett.* **331**, 322–334 (2012).
34. M. A. Berke *et al.*, *Quat. Sci. Rev.* **55**, 59–74 (2012).
35. J. G. Charney, *Q. J. R. Meteorol. Soc.* **101**, 193–202 (1975).
36. J. Shukla, Y. Mintz, *Science* **215**, 1498–1501 (1982).
37. A. Parker *et al.*, *J. Quaternary Sci.* **19**, 665–676 (2004).
38. C. Zhang, *J. Clim.* **6**, 1898–1913 (1993).
39. E. Black, J. Slingo, K. R. Sperber, *Mon. Weather Rev.* **131**, 74–94 (2003).
40. J. E. Tierney, J. E. Smerdon, K. J. Anchukaitis, R. Seager, *Nature* **493**, 389–392 (2013).
41. A. Chakraborty, S. K. Behera, M. Mujumdar, R. Ohba, T. Yamagata, *Mon. Weather Rev.* **134**, 598–617 (2006).
42. Y. Zhao *et al.*, *Clim. Dyn.* **25**, 777–800 (2005).
43. F. Rostek, E. Bard, L. Beaufort, C. Sonzogni, G. Ganssen, *Deep Sea Res. Part II Top. Stud. Oceanogr.* **44**, 1461–1480 (1997).
44. P. Anand *et al.*, *Paleoceanography* **23**, PA4207 (2008).
45. M. Mohtadi, S. Steinke, A. Lückge, J. Groeneveld, E. Hathorne, *Earth Planet. Sci. Lett.* **292**, 89–97 (2010).
46. E. Kalnay *et al.*, *Bull. Am. Meteorol. Soc.* **77**, 437–471 (1996).

Acknowledgments: This study was supported by National Science Foundation grant OCE-1203892 to J.E.T., National Oceanic and Atmospheric Administration award NAO80AR4320912 to P.B.d.M., and the Lamont-Doherty Earth Observatory (LDEO) Climate and Life Initiative. We thank E. Hamilton and C. Johnson for assistance with the stable isotope measurements; J.-B. Stuut, G. Ganssen, and C. Cleroux for assistance with core sampling; J. Fang and T. Guilderson for assistance with the radiocarbon dating; and C. Ummenhofer for comments on the initial versions of the manuscript. We thank the Captain and crew of the *R/V Pelagia* for their remarkable professionalism during the penultimate leg (Cruise 178; April to May 2001) of the scientific circumnavigation of the African continent. With co-chief scientist G. Ganssen, we were able to obtain valuable samples from this remote and geopolitically challenging region. This is LDEO contribution number 7739.

Supplementary Materials

www.sciencemag.org/content/342/6160/843/suppl/DC1
Materials and Methods
Figs. S1 to S3
Tables S1 and S2
References

13 May 2013; accepted 26 September 2013
Published online 10 October 2013;
10.1126/science.1240411

Dosage Compensation via Transposable Element Mediated Rewiring of a Regulatory Network

Christopher E. Ellison and Doris Bachtrog*

Transposable elements (TEs) may contribute to evolutionary innovations through the rewiring of networks by supplying ready-to-use cis regulatory elements. Genes on the *Drosophila* X chromosome are coordinately regulated by the male specific lethal (MSL) complex to achieve dosage compensation in males. We show that the acquisition of dozens of MSL binding sites on evolutionarily new X chromosomes was facilitated by the independent co-option of a mutant helitron TE that attracts the MSL complex (TE domestication). The recently formed neo-X recruits helitrons that provide dozens of functional, but suboptimal, MSL binding sites, whereas the older XR chromosome has ceased acquisition and appears to have fine-tuned the binding affinities of more ancient elements for the MSL complex. Thus, TE-mediated rewiring of regulatory networks through domestication and amplification may be followed by fine-tuning of the cis-regulatory element supplied by the TE and erosion of nonfunctional regions.

Active transposable elements (TEs) impose a substantial mutational burden on the host genome (*1*–*4*). However, there is growing evidence implicating TEs as drivers of key evolutionary innovations by creating or rewiring regulatory networks (*5*–*11*). Many TEs harbor a variety of regulatory motifs, and TE amplification may allow for the rapid accumulation of a specific motif throughout the genome, thus recruiting multiple genes into a single regulatory network (*12*).

In *Drosophila miranda*, multiple sex chromosome/autosome fusions have created a series of X chromosomes of differing ages (Fig. 1). The ancestral X chromosome, XL, is homologous to the *D. melanogaster* X and is at least 60 million years old (*13*). Chromosome XR became a sex chromosome ~15 million years ago and is shared among members of the *affinis* and *pseudoobscura* subgroups, whereas the neo-X chromosome is specific to *D. miranda* and originated only 1 million years ago (*14*, *15*). The male specific lethal (MSL) complex coordinates gene expression on the *Drosophila* male X to achieve dosage compensation (*16*). This complex is recruited to the X chromosome in males to high-affinity chromatin entry sites (CES) containing a conserved, roughly 21–base

Department of Integrative Biology, University of California, Berkeley, Berkeley, CA 94720, USA.
*Corresponding author. E-mail: dbachtrog@berkeley.edu

www.sciencemag.org/content/full/science.1240411/DC1

Supplementary Material for

Abrupt Shifts in Horn of Africa Hydroclimate Since the Last Glacial Maximum

Jessica E. Tierney,* Peter B. deMenocal

*Corresponding author. E-mail: tierney@whoi.edu

Published 10 October 2013 on *Science* Express
DOI: 10.1126/science.1240411

This PDF file includes:

1. Core site & sediment provenance

Marine sediment core P178-15P was collected from the Gulf of Aden at 11° 57.3' N, 44° 18' E, 869 meters water depth from the *R/V Pelagia* in 2001. Site P178-15P receives a substantial amount of aeolian terrestrial material that primarily derives from the Horn of Africa: TOMS aerosol index data (*1*) indicate that the Gulf of Aden receives nearly all of its dust from May–August, when southwesterly winds deliver dust from the Horn region (Fig. S1).

2. Leaf wax hydrogen isotopic analysis

Core P178-15P was subsampled for hydrogen isotopic analyses with an average resolution of 10 cm and at a resolution of 4 cm near critical transitions. Wet sediments were freeze-dried, homogenized, and then approximately 12–18 grams were extracted using an accelerated solvent extractor (ASE) 350 at a temperature of 100°C and maximum pressure of 1500 psi. The resulting total lipid extracts (TLEs) were evaporated to dryness then further purified using column chromatography. TLEs were first separated into neutral and acid fractions over LC-NH_2 gel using CH_2Cl_2:isopropanol (2:1) and 4% acetic acid in ethyl ether as the respective eluents. The acid fraction was then methylated (heated to 50°C, overnight) using acetyl chloride-acidified GC grade methanol of a known isotopic composition. The methylated fatty acids (fatty acid methyl esters; FAMEs) were then further purified over silica gel using hexane and CH_2Cl_2 as respective eluents. The CH_2Cl_2 fraction, containing the FAMEs, was dried under N_2 gas and then redissolved in hexane for analysis.

The hydrogen isotopic composition of the FAMEs was measured via gas chromatography-pyrolysis-isotope ratio monitoring mass spectrometry (GC-IR-MS) using a Thermo Finnigan Delta V Plus mass spectrometer at Lamont-Doherty Earth Observatory. H_2 gas calibrated to an authentic FAME standard ("F8", provided by Arndt Schimmelmann at Indiana University) was used as a working reference for each analysis. In addition, an internal standard (eicosenoic acid) added to each sample after extraction but before purification and an external synthetic FAME standard measured every sixth analysis were used to monitor machine drift. All samples were run in duplicate and a select number were run in triplicate. The standard error of repeat analyses was 1.5‰.

We focused on analyzing the C_{30} fatty acid as the representative terrestrial leaf wax due to evidence that fatty acids of shorter chain lengths could potentially have a competing aquatic origin in the marine environment (*2*). Low abundances precluded collecting C_{32} fatty acid data for comparison.

To isolate variance associated with the regional hydrological cycle, we removed the effect of changing ice volume on the isotopic composition of $\delta\mathrm{D}_{wax}$ prior to plotting the data in Figures 2 and 3. To estimate the ice volume effect, we assumed a Last Glacial Maximum change in global δ^{18}O of 1‰ (*3*) and scaled the benthic oxygen isotope stack (*4*) – a proxy for the changes in global ice volume – accordingly. We then removed the ice volume change from the data using the following equation:

$$\delta D_{wax-corr} = \frac{1000 + \delta D_{wax}}{8 \times 0.001 \times \delta^{18}O_{ice} + 1} - 1000 \quad (1)$$

For consistency, we corrected the Lake Tanganyika and Lake Challa $\delta\mathrm{D}_{wax}$ data in the same fashion.

3. Age modeling

We used 20 accelerated mass spectrometry (AMS) radiocarbon dates (analyzed at Lawrence Livermore National Laboratory) to construct a chronology for core P178-15P (Table 1). The ^{14}C date near the top of the core (5.5 cm) yielded a date (475 ^{14}C year) that once corrected for the global and local marine reservoir would suggest a "postbomb" (>1950 AD) age (Table S1) and thus was not explicitly calibrated but rather used to place a uniform prior on the coretop age of 1950–2001 AD (year of collection). Radiocarbon dates were converted to calendar age probability distributions using the P_Sequence routine in OxCal 4.1 (*5, 6*). We employed the Marine09 curve (*7*) and used a prior on the local reservoir correction (ΔR) of 188 $\pm$ 73, the weighted average and standard deviation of seven ΔR estimates from the Gulf of Aden region (*8, 9*). OxCal's P_Sequence models sedimentation as a monotonic Poisson process (*6*) with a user-specified step size (k, an inverse value). We set k to 0.25, which provides a high level of flexibility in the model and nearly approximates the Sequence routine, which does not use depth information (*6*). The resulting posterior distributions of the calibrated ^{14}C dates therefore assume superposition but place only minimal constraints on changes in the sedimentation rate.

Using the posterior probability distributions of each calibrated date, we constructed 5,000 possible age-depth models using a monotonic Monte Carlo method (*10*). No further assumptions about sedimentation rate are made in this process. The resulting ensemble of age models is used to estimate the median, 68% and 95% uncertainty bounds for each depth interval at which a proxy measurement was made and to form the empirical midpoint and duration probability distributions for identified transitions (see below). The analytical uncertainty of the isotopic measurements (1.5‰, 1σ) is compounded with the time uncertainty in order to plot the error

bars in Figures 2 and 3 of the main text.

To enable consistent cross-site comparison, we recalibrated the Lake Tanganyika ^{14}C dates listed in ref. (*11*) (previously calibrated with IntCal04) and modeled the age-depth relationship using the same OxCal–Monte Carlo process. However, as Tanganyika is a terrestrial record, we used the IntCal09 curve instead of Marine09. We accounted for the evolving lake ^{14}C reservoir in the same fashion as previous work (*11, 12*), by fitting a linear regression to the paired bulk-macrofossil dates to estimate the ^{14}C age – reservoir age relationship from the LGM to the late Holocene. We then compounded the regression uncertainty with the analytical ^{14}C uncertainty prior to calibration with OxCal.

The Lake Challa record employs a radiocarbon-based age model based on a tailored Bayesian process designed to simultaneously account for an evolving lake reservoir and the large amount of ^{14}C dates analyzed on this core (*13*). A series of splines were then fit to the resulting posterior age distributions to generate uncertainty bounds for each analyzed depth interval in the core (*13*). Rather than repeating this process and risk violating the specific assumptions of this age model, we simply resampled the age uncertainty bounds determined in ref. (*13*) using a Monte Carlo process to generate the needed 5,000 age model iterations.

4. Identification and analysis of transitions

Although the transitions of interest are visually apparent (cf. Fig. 3) two quantitative methods were used to ascertain the location and duration of the transitions. First, a changepoint detection algorithm (*14*) was used to confirm the presence and location of significant regime shifts in the Gulf of Aden, Lake Tanganyika, and Lake Challa proxy data by both core depth and median age. The changepoint algorithm detected changepoints corresponding to the Heinrich Event 1 (H1), Younger Dryas (YD), and mid-Holocene terminations in the Gulf of Aden and Tanganyika data but only detected changepoints corresponding to the YD, and mid-Holocene terminations in Lake Challa $\delta\mathrm{D}_{wax}$. This result corroborates the visual assessment that there is no clear H1 signature in the Lake Challa $\delta\mathrm{D}_{wax}$. Although $\delta\mathrm{D}_{wax}$ (*15*), lake level inferences (*16*), and organic geochemical indicators (*17*) all suggest that the Challa area was drier during the late glacial period (20–15 ka) following a relatively wet Last Glacial Maximum, aside from a possible brief lowstand (*16*) there is little evidence of an H1 response. The lack of a strong H1 response at this location may be related to large-scale changes in the Indian Ocean Walker circulation during the LGM, which resulted in relatively wet conditions along the southeast African coast (*18*).

Next, the SiZer method (significant zero crossings of the derivatives) (*19*) was used to determine the start- and end-points of each transition. SiZer was applied to the data by both depth and median age to check for consistency. SiZer applies a series of Gaussian smoothings to the data and then searches for the start and endpoint of trends, which are defined as the interval at which the null hypothesis of no trend can be rejected at the level of $p < 0.05$. In all cases the detected changepoints fell within the bounds of the SiZer analysis, and no H1–B/A trend was detected in the Lake Challa time series, consistent with the changepoint results. The identified start- and end-points are listed in Table 2. Once the start and end of the transitions were identified by depth, the duration ($T_{start} - T_{end}$) and midpoint timing ($T_{start} - T_{end}/2$) of each transition was determined for each of the 5,000 Monte Carlo age models produced by the process described in Section 2. The resulting values were then used to construct the empirical probability distributions shown in Figures 3 and 4 and to estimate the 2σ uncertainty values given in the main text.

The median observed duration of the transitions has a strong relationship ($r = 0.95$; Pearson correlation) with the sampling interval (ΔT) of the proxy over the transition (Fig. S2) with a higher sampling interval corresponding to a longer duration. This is expected, as the duration of the original event will be appear to be longer in proxy records where a combination of low sedimentation rates, mixing (bioturbation) processes, and the sampling rate of the proxy attenuates the signal. Interestingly, the relationship between the inverse of the sedimentation rate and duration is not as strong ($r = 0.66$, Fig. S2) suggesting that in this case the sampling rate has a bigger effect on the observed duration than sedimentation rate. Thus, the observed durations are in themselves maximum estimates of the true duration of the climate event. To provide a simple first-order estimate a "theoretical" duration of the transitions (e.g., what the duration may be sans sedimentation and sampling effects) we used ordinary least squares linear regression to estimate the slope of the sampling interval effect and then remove that slope change from the data ($R + \alpha$ where R = residuals, observed-predicted; and α = y-intercept). We performed this regression and calculation iteratively to fully sample the uncertainty bounds of the duration and sampling interval data (Fig. S2) and produce the theoretical probability distributions in Figure 4.

Table 2 lists the locations of the detected changepoints (by core depth), the start and end of the transitions (by core depth), the median and standard deviation of the sampling interval across the transition, the median and standard deviation of the duration and midpoint value, and the median and standard deviation of the theoretical duration.

5. Leaf wax carbon isotopes

The carbon isotopic signature of leaf waxes ($\delta^{13}C_{wax}$) reflects the carbon isotopic composition of the bulk plant tissue (*20*) which is determined by the metabolic pathway of the source plants (e.g., C_3 vs. C_4, each associated with distinctive carbon isotopic fractionations) (*21*) as well as the ratio of CO_2 concentration within the leaves to that in atmosphere (c_i/c_a ratio). The c_i/c_a ratio is determined by the stomatal aperture, which is sensitive to a number of environmental factors including precipitation, humidity, light intensity, and atmospheric pCO_2 (*22*). Therefore, $\delta^{13}C_{wax}$ acts as an indicator of vegetation type in the landscape (especially in regions where there is a mix of C_3 vs. C_4 plants) but can also reflect a complex combination of environmental influences. In tropical Africa, soil carbon isotopes reliably track landscape types (e.g., grassland, shrubland, forest) (*23, 24*) and it is assumed that $\delta^{13}C_{wax}$ can similarly provide insight into past landscape changes (*25*).

Different types of plants (e.g., grass vs. tree) have slightly different "apparent" hydrogen isotopic fractionations (ε, i.e., the observed difference between δD_P and δD_{wax}) (*26*). As these are empirical observations, is not clear whether they are attributable to physiological or climatic factors; most likely, they reflect a combination of both (*26*). If the differences in apparent ε are related to physiological differences between plants, then changes in the vegetation type from which the waxes derive over time could influence the δD_{wax} signature independently of climatic change, and of particular concern here, could influence the abruptness of a hydroclimate transition as it is recorded by δD_{wax}. Insofar as $\delta^{13}C_{wax}$ is a proxy for vegetative cover, it can be used to assess whether or not vegetation changes could have influenced δD_{wax}; however, it should be noted that, because $\delta^{13}C_{wax}$ is in of itself sensitive to aridity, some relationship is expected. $\delta^{13}C_{wax}$ data is available at all three of the sites investigated here. At Lake Tanganyika and Lake Challa, carbon isotopes were previously measured on the leaf waxes to infer past changes in vegetation (*27, 28*). We also measured $\delta^{13}C_{wax}$ in the Gulf of Aden core at a lower resolution to compare changes in $\delta^{13}C_{wax}$ with δD_{wax}.

While the trajectory of the δD_{wax} data at the three sites is relatively similar, the $\delta^{13}C_{wax}$ data suggest that the vegetative cover at each site evolved differently (Figure S2). In the Gulf of Aden record, the small range of $\delta^{13}C_{wax}$ values (-24 to -28‰) suggests a relatively stable landscape consisting of C_4 grasses and C_3 shrubs, similar to today's vegetation across the Horn of Africa. The Heinrich Event 1 and mid-Holocene transitions are accompanied by small 1.5 ‰ shifts in $\delta^{13}C_{wax}$ towards more depleted values, but no shift is observed at the termination of the Younger Dryas (YD) and onset of the African Humid Period (AHP). Moreover, $\delta^{13}C_{wax}$ seems to trend towards more enriched values shortly after reaching minimum values during the

Bölling-Allerød period and does not change in response to the AHP. Therefore, it is unlikely that shifts in vegetation influenced the δD_{wax} record at this site, and furthermore, the evolution of $\delta^{13}C_{wax}$ seems to be only partially linked to aridity.

At Lake Tanganyika, the range in $\delta^{13}C_{wax}$ is large (-27 to -40‰) indicating a substantial change in the landscape from a mixed woodland/grassland ($\delta^{13}C_{wax}$ values of -27 to -32‰) that characterizes the modern and late glacial landscapes to a humid forest ($\delta^{13}C_{wax}$ values of -34 to -40‰) during the early Holocene. Pollen data corroborate this change in the vegetation, indicating an expansion of mesic forests during the early Holocene (*27*). However, the shifts between each ecosystem are not perfectly coeval with the changes in δD_{wax}. The H1 and YD terminations are not accompanied by a corresponding shift in $\delta^{13}C_{wax}$ and, as with the Gulf of Aden record, $\delta^{13}C_{wax}$ becomes gradually more enriched across the Holocene rather than remaining at forest-type values throughout the AHP. Therefore, it is unlikely that vegetation change here influenced the timing and severity of the transitions in δD_{wax} directly (i.e., by altering apparent ε).

At Lake Challa, $\delta^{13}C_{wax}$ spans a broader range (-32 to -22 ‰) than in the Gulf of Aden record, but does not approach values that would indicate the establishment of forest. Unlike the Gulf of Aden and Tanganyika data, which suggest that late glacial and modern vegetation were relatively similar, $\delta^{13}C_{wax}$ at Challa suggests that a late-glacial C_4 grass-dominated landscape was replaced by woodland beginning in the Early Holocene and that this vegetation type persisted until the present. There is no change in $\delta^{13}C_{wax}$ across the mid-Holocene transition. There is, however, a distinct enrichment in $\delta^{13}C_{wax}$ during the Younger Dryas event suggestive of a re-establishment of grassland (Fig. S2). As grasses have a more negative apparent fractionation than woody plants (*26*), a shift to grasslands would be expected to bias δD_{wax} towards more negative values. As δD_{wax} instead records a strong enrichment during the YD in accordance with an aridity response, it would seem that the vegetation change has little apparent influence on δD_{wax}.

Overall, the diversity of vegetation and landscape evolution at the three sites suggested by the $\delta^{13}C_{wax}$ data rules out the possibility that the magnitude or abruptness of the δD_{wax} data is primarily a consequence of vegetation change. Incidentally, the $\delta^{13}C_{wax}$ data also imply that the abruptness of the transitions cannot be confidently attributed to strong vegetation feedbacks, with the possible exception of the onset and termination of the AHP in Lake Tanganyika, where the dramatic transition from woodland to forest and back to woodland would have been associated with a large change in surface albedo.

References

1. R. D. McPeters, P. K. Bhartia, A. J. Krueger, O. Torres, J. R. Herman, *NASA Technical Publication* **1998-206895** (1998).
2. S. Kusch, J. Rethemeyer, E. Schefuß, G. Mollenhauer, *Geochimica et Cosmochimica Acta* **74**, 7031 (2010).
3. D. P. Schrag, G. Hampt, D. W. Murray, *Science* **272**, 1930 (1996).
4. L. E. Lisiecki, M. E. Raymo, *Paleoceanography* **20**, PA1003 (2005).
5. C. Bronk Ramsey, *Radiocarbon* **37**, 425 (1995).
6. C. Bronk Ramsey, *Quat. Sci. Rev.* **27**, 42 (2008).
7. P. J. Reimer, *et al.*, *Radiocarbon* **51**, 1111 (2009).
8. R. Cember, *J. Geophys. Res.* **94**, 2111 (1989).
9. J. Southon, M. Kashgarian, M. Fontugne, B. Metivier, W. Yim, *Radiocarbon* **44**, 167 (2002).
10. K. J. Anchukaitis, J. E. Tierney, *Climate Dynamics* pp. 1–16 (2012).
11. J. E. Tierney, *et al.*, *Science* **322**, 252 (2008).
12. A. A. Felton, *et al.*, *Palaeogeog. Palaeoclimatol. Palaeoecol.* **252**, 405 (2007).
13. M. Blaauw, *et al.*, *Quaternary Science Reviews* **30**, 3043 (2011).
14. S. Rodionov, *Geophysical Research Letters* **31**, L09204 (2004).
15. J. E. Tierney, J. M. Russell, J. S. Sinninghe Damsté, Y. Huang, D. Verschuren, *Quat. Sci. Rev.* **30**, 798 (2011).
16. J. Moernaut, *et al.*, *Earth Planet. Sci. Lett.* **290**, 214 (2010).
17. D. Verschuren, *et al.*, *Nature* **462**, 637 (2009).
18. P. N. DiNezio, J. E. Tierney, *Nature Geoscience* p. in press (2013).
19. P. Chaudhuri, J. S. Marron, *Journal of the American Statistical Association* **94**, 807 (1999).
20. J. W. Collister, G. Rieley, B. Stern, G. Eglinton, B. Fry, *Org. Geochem.* **21**, 619 (1994).
21. M. H. O'Leary, *Phytochemistry* **20**, 553 (1981).
22. G. D. Farquhar, J. R. Ehleringer, K. T. Hubick, *Annual review of plant biology* **40**, 503 (1989).
23. T. Cerling, J. Quade, Y. Wang, J. Bowman, *Nature* **341**, 138 (1989).
24. T. E. Cerling, *et al.*, *AGU Fall Meeting Abstracts* (2010), vol. 1, p. 08.

25. C. R. Magill, G. M. Ashley, K. H. Freeman, *Proceedings of the National Academy of Sciences* **110**, 1175 (2013).

26. D. Sachse, *et al.*, *Annu. Rev. Earth Planet. Sci.* **40**, 221 (2012).

27. J. E. Tierney, J. M. Russell, Y. Huang, *Quat. Sci. Rev.* **29**, 787 (2010).

28. J. S. Sinninghe Damsté, *et al.*, *Earth and Planetary Science Letters* **302**, 236 (2011).

Table S1. Radiocarbon dates on P178-15P, analyzed at Lawrence Livermore National Laboratory, and OxCal calibrated ages.

CAMS #	Depth (cm)	^{14}C Age	Error (1σ)	Median Calibrated Age (BP)	Error (1σ)
152757	5.5	475	30	$<$0	N/A
152758	41.5	1565	30	916	46
152759	90.5	2465	30	1868	49
152760	150.5	3030	35	2649	55
152761	200.5	4395	30	4292	62
156467	220.5	4765	35	4790	59
152762	260.5	5485	30	5640	42
156468	340.5	6790	35	7143	57
152763	420.5	9430	35	10036	80
156469	460.5	10045	40	10794	112
152764	520.5	11730	40	13020	85
156470	560.5	12910	45	14557	265
159387	580.5	14160	40	16721	109
156471	600.5	15370	70	17886	146
152765	640.5	16570	60	19264	122
159388	680.5	21150	70	24526	171
156472	700.5	23160	160	26963	307
156473	780.5	27170	260	31104	162
156474	840.5	29180	340	33901	454
152766	900.5	34930	450	38372	667

Table S2. Location, timing, and duration of analyzed transitions. Listed uncertainties are 2σ. Changepoint = location of the detected regime shifts using the algorithm of ref. (*14*). Start and end-points are informed by SiZer analysis (*19*).

Name	Changepoint (cm)	Start (cm)	End (cm)	Sampling Interval (yr)	Timing (yr)	Observed Duration (yr)	Theoretical Duration (yr)
Gulf of Aden							
Mid-Holocene	210.5	250.5	210.5	130 ± 17	4930 ± 74	916 ± 118	375 ± 61
Younger Dryas	480.5	484.5	434.5	253 ± 42	10849 ± 135	1263 ± 211	219 ± 75
Heinrich Event 1	568.5	572.5	540.5	435 ± 50	14675 ± 301	2177 ± 252	377 ± 83
Lake Tanganyika							
Mid-Holocene	84.5	116.5	74.5	143 ± 39	5066 ± 154	1286 ± 348	698 ± 191
Younger Dryas	258	265	247	87 ± 24	11601 ± 208	609 ± 168	250 ± 80
Heinrich Event 1	331	341	322	274 ± 46	15763 ± 446	1643 ± 277	510 ± 79
Lake Challa							
Mid-Holocene	470	470	374	299 ± 19	5023 ± 264	1494 ± 94	260 ± 69
Younger Dryas	974	986	926	98 ± 19	11604 ± 356	687 ± 135	281 ± 67

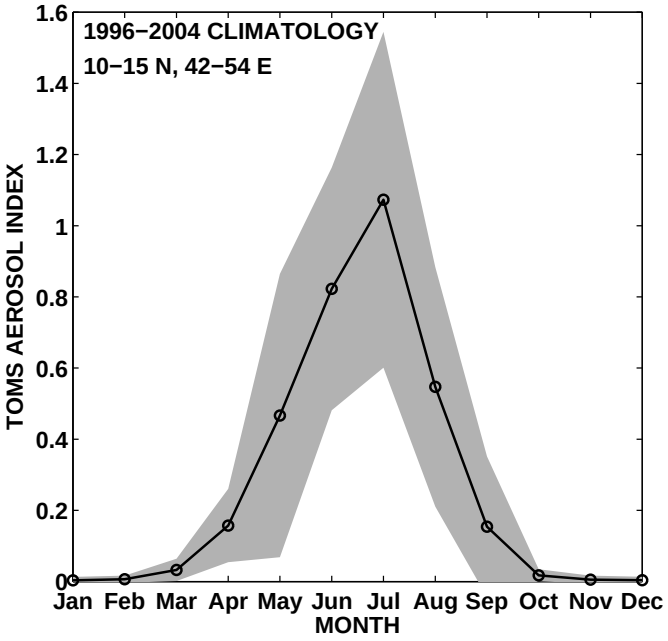

Figure S1. TOMS (Total Ozone Mapping Spectrometer) EPTOMS aerosol index (dimensionless) data over the Gulf of Aden (10–15N, 42–54E), 1996–2004 climatology (*1*).

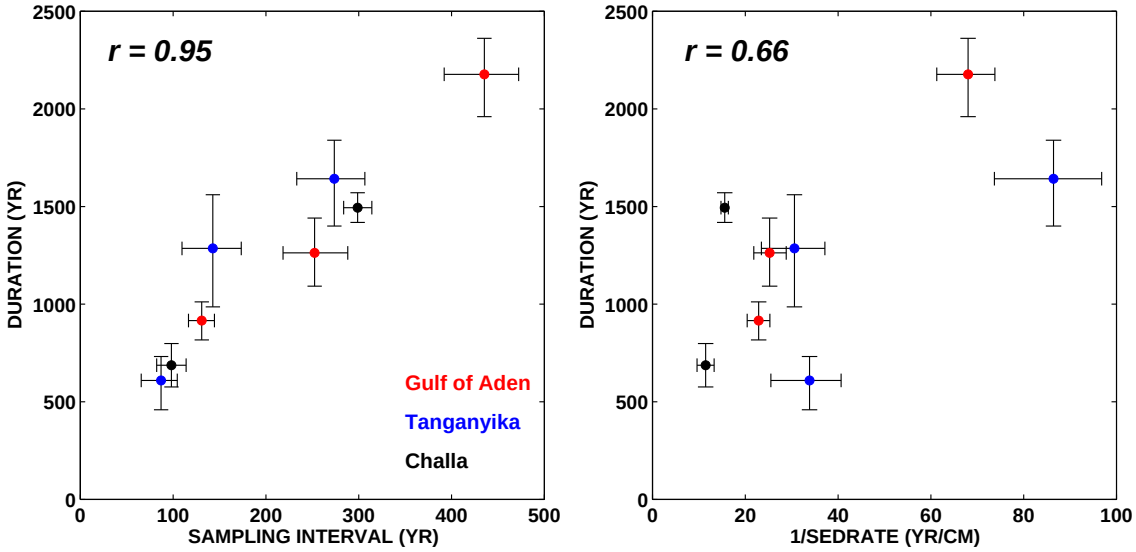

Figure S2. At left, the relationship between the sampling interval of the proxy (ΔT) and the duration of the transition, for all eight analyzed transitions at three different sites. At right, the relationship between the inverse sedimentation rate ($\Delta T/\Delta depth$) and the duration of the transition, for all eight analyzed transitions at three different sites. r values represent Pearson correlation coefficients. Error bars indicate the empirical 90% confidence intervals based on the Monte Carlo age resampling procedure.

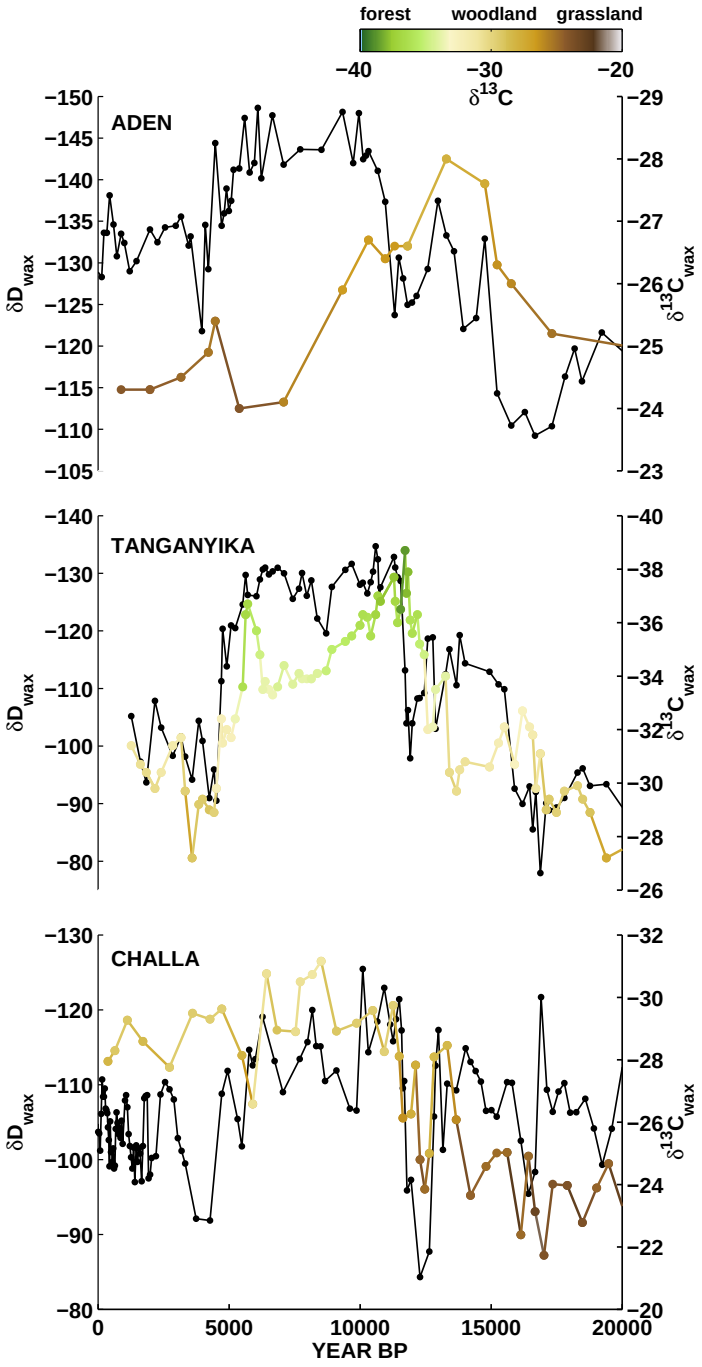

Figure S3. $\delta^{13}C_{wax}$ (color coded by value to illustrate associated landscapes) compared to δD_{wax} (in black) at each of the three East African sites. Note different y-axes scales for each site. Colorbar shows approximate landscape types associated with given $\delta^{13}C_{wax}$values, as in ref. (*25*).

CLIMATE CHANGE

Out of the African Humid Period

Edouard Bard

Data from an East African marine core help to explain the transition from the more humid conditions in the early Holocene to today's arid climate.

During the last deglaciation, climatic changes allowed human societies to develop and flourish in the subtropical zone from North Africa to Asia. On page 843 of this issue, Tierney and deMenocal (*1*) report details of these climatic changes in North Africa. They show that between 21,000 and 11,500 calendar years before present (cal. yr B.P.), millennium-long periods of subtropical aridity corresponded to transient phases of intense iceberg melting into the North Atlantic. The Holocene period, starting ~11,500 cal. yr B.P., was characterized by a prominent increase in rainfall triggered by summer insolation values higher than those of today. The spatial extent and temporal limits of this period, called the African Humid Period in North Africa, are still debated (see the figure).

From the early Holocene to the present day, summer insolation in the subtropical zone has slowly decreased as a result of changes in Earth's orbit around the Sun. This gradual change over 10 millennia contrasts with the complexity of rainfall proxy observations gathered from marine coastal sediments, lake sediments, and cave stalagmites. The African Humid Period ended abruptly ~5000 cal. yr B.P. in many locations, such as western North Africa (*2*, *3*) and northern Kenya (*4*). In other places, changes occurred gradually over several millennia—for example, in the central Sahara (*5*) and the southern Arabian Peninsula (*6*).

The increasingly arid conditions at the end of the African Humid Period forced human agropastoral societies to improve their organization in order to optimize natural resources, in particular freshwater supplies (*7*). As a result of growing demographic pressure in an environment that was again becoming hostile, Neolithic communities were forced to concentrate in river valleys and to develop irrigation systems. These complex transformations help explain the rise of the Egyptian, Sumerian, and Harappan civilizations that flourished along major rivers such as the Nile, Euphrates, Tigris, and Indus.

Climate projections for the next century show that the subtropical zone is likely to experience major rainfall changes (*8*). It is thus crucial to understand how some ancient societies could adapt through technical and political innovations, whereas other human groups were forced to migrate. The spatial variability of the mid-Holocene arid transition provides a further complication. The exposure of some Neolithic societies to a stronger climatic forcing than others may explain their different fates: success and domination, or collapse and exodus.

Why was there so much spatial variability at the end of the African Humid Period? The prevailing theory is that the disappearance of vegetation accelerated the drying of the continent through regional changes of albedo, water storage in roots and soils, and evapotranspiration by plants. Simulations with climate models representing the vegetation and its effect on regional climate (*9*) suggest that the efficiency of this biogeophysical feedback may have varied with longitude, which would be compatible with observations. In some places, vegetation diversity may have promoted a gradual termination of the African Humid Period (*10*).

However, Tierney and deMenocal show that the biogeophysical feedback may not be the only cause of the abrupt climate response, particularly in regions that were not covered by abundant vegetation in the early Holocene. This was probably the case for the northeastern corner of Africa, which prompted Tierney and deMenocal to look for a new record from the Horn of Africa. In a marine sediment core from the Gulf of Aden (see the figure), they analyzed leaf waxes transported by winds from the African continent. This site is under the double influence of the African climate and the Indian Ocean, with its summer monsoon winds bringing moisture to the region and picking up dust

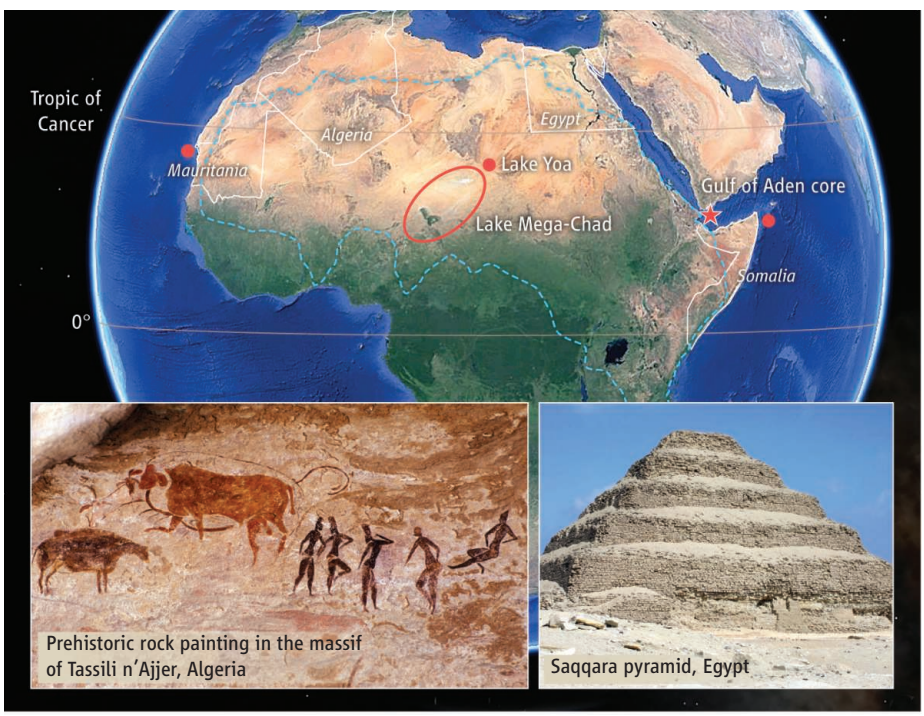

North African climate, then and now. The Landsat image shows modern forests in green and sandy and rocky deserts in yellow and brown. During the African Humid Period ~11,500 to 5000 years ago, this region was much more humid, as shown by the contours (dashed line) marking the zone of high water levels (*15*). Tierney and deMenocal have studied a sediment core from the Gulf of Aden that provides detailed insights into the beginning and end of the African Humid Period. The work complements previous studies of sediment cores taken off the coasts of Mauritania (*2*, *3*) and Somalia (*11*) and from Lake Yoa (*5*, *12*) and Lake Chad (*14*). The African Humid Period and its termination affected human civilizations, as illustrated by a rock painting from the Tassili n'Ajjer, Algeria, and the pyramid of pharaoh Djoser in Saqqara, Egypt.

Collège de France and CEREGE (Aix-Marseille University, CNRS, IRD, CdF), Aix-en-Provence F-13545, France. E-mail: bard@cerege.fr

Published by AAAS

over the East African continent. In a nearby deep-sea sediment core off the Somalian coast, Holocene aridification over the course of 2000 years was recorded from the radiogenic isotope signature of wind-transported dust (*11*). Tierney and deMenocal instead measured the deuterium-to-hydrogen ratio (D/H) of the leaf waxes; this ratio is directly linked to the isotopic composition of precipitation and hence to total rainfall.

By comparing their Gulf of Aden record with published records, Tierney and deMenocal conclude that the African Humid Period ended abruptly within a few centuries and was synchronous in the western and eastern part of Africa. By considering modern climate observations and model simulations, they propose that East African rainfall responded in a nonlinear way to surface temperatures in the Indian Ocean.

Tierney and deMenocal's Gulf of Aden record provides key information for understanding North African climate during the Holocene. However, much research is still needed to build a comprehensive view of hydroclimatic changes during the African Humid Period. Most published records are based on proxies that are difficult to link unequivocally to rainfall changes. For example, records of wind-transported material reflect both the decrease in vegetation cover and the increase in the dust source area caused by widespread lake desiccation. Documenting these parameters requires information from multiple proxies measured in the same continental or marine archives. The time resolution of records must also be improved by increasing the sampling rate for these proxies. Decadal-to-seasonal profiles measured with geochemical scanners (*12*) allow studying African Humid Period transitions without relying on statistical corrections.

More continuous records are needed from north of the Gulf of Aden, along the Nile Valley and the Red Sea. Obtaining new data from central North Africa is also crucial for backing up observations made in sediments of the small Lake Yoa (*5*, *12*). Of particular importance is the Holocene history of Lake Chad, which was at least 10 times as large during the African Humid Period than it is today (*13*). Pollen data from Lake Chad (*14*) indicate that vegetation changes occurred progressively over about two millennia, but that century-scale variability was superimposed on the mid-Holocene drying trend. Additional proxies remain to be measured and longer continuous cores to be collected and studied from Lake Chad to advance understanding of the African Humid Period.

References

1. J. E. Tierney, P. B. deMenocal, *Science* **342**, 843 (2013); 10.1126/science.1240411.
2. P. B. deMenocal *et al.*, *Quat. Sci. Rev.* **19**, 347 (2000).
3. D. McGee, P. B. deMenocal, G. Winckler, J. B. W. Stuut, L. I. Bradtmiller, *Earth Planet. Sci. Lett.* **371-372**, 163 (2013).
4. Y. Garcin, D. Melnick, M. R. Strecker, D. Olago, J.-J. Tiercelin, *Earth Planet. Sci. Lett.* **331**, 322 (2012).
5. S. Kröpelin *et al.*, *Science* **320**, 765 (2008).
6. D. Fleitmann *et al.*, *Quat. Sci. Rev.* **26**, 170 (2007).
7. R. Kuper, S. Kröpelin, *Science* **313**, 803 (2006).
8. Intergovernmental Panel on Climate Change, Working Group I Contribution to the IPCC Fifth Assessment Report, T. Stocker *et al.*, Eds. (World Meteorological Organization and United Nations Environment Programme, Geneva, Switzerland, 2013).
9. V. Brovkin, M. Claussen, *Science* **322**, 1326 (2008).
10. M. Claussen, S. Bathiany, V. Brovkin, T. Kleinen, *Nat. Geosci.* 10.1038/ngeo1962 (2013).
11. S. Jung, G. R. Davies, G. M. Ganssen, D. Kroon, *Earth Planet. Sci. Lett.* **221**, 27 (2004).
12. P. Francus *et al.*, *Sedimentology* **60**, 911 (2013).
13. M. Schuster *et al.*, *Quat. Sci. Rev.* **24**, 1821 (2005).
14. P. G. C. Amaral *et al.*, *Clim. Past* **9**, 223 (2013).
15. N. Roberts, *The Holocene, An Environmental History* (Blackwell, Oxford, 1998).

10.1126/science.1246519

CANCER

Potential of the Synthetic Lethality Principle

Elucidating the first principles of synthetic lethality in cancer, including biological context, will assist clinical translation.

Sebastian M. B. Nijman[1] and Stephen H. Friend[2]

Most cancer mutations, including those causing a loss of function, are not directly "druggable" with conventional small-molecule drugs or biologicals, such as antibodies. Thus, despite our growing knowledge of mutations that drive cancer progression, there remains a frustrating gap in translating this information into the development of targeted treatments that kill only cancer cells. An approach that exploits a concept from genetics called "synthetic lethality" could provide a solution. But it has been over 15 years since that framework was proposed (*1*). Does the synthetic lethality principle still have the potential for treating cancer?

Synthetic lethality, first observed in the fruit fly *Drosophila melanogaster* almost a century ago, describes a phenomenon where only the simultaneous perturbation of two genes results in a deadly combination. Thus, cancer aberrations that are not readily targetable [e.g., tumor suppressor proteins such as retinblastoma protein 1 (RB1) and p53 (*TP53*); oncogenes such as *RAS* and c-*MYC*] could be indirectly exploited by inhibiting the product of another gene (*2*–*4*). The broader definition of synthetic lethality has also been referred to as "nononcogene addiction" or "induced essentiality" to distinguish it from its classical meaning in genetics. In the budding yeast *Saccharomyces cerevisiae*, most genes display numerous synthetic lethal interactions (*5*, *6*), which may also apply to many human cancer genes. Furthermore, "passenger" mutations, which do not directly contribute to tumorigenesis, and even rewiring of cellular networks that give rise to a cancerous state, may also be exploited with the synthetic lethal principle. However, to date, only a single synthetic lethal interaction has shown therapeutic promise. Why have synthetic lethal therapies largely failed to deliver?

The proof of principle that the synthetic lethality concept is clinically translatable is the efficacy of drugs that target the single-strand DNA repair enzyme poly(ADP-ribose) polymerase (PARP) in tumors with mutations in the *BRCA1* and *BRCA2* genes (*7*). These genes encode tumor suppressor proteins that help repair damaged DNA. The remarkable ability of tumors to acquire resistance to PARP inhibitors by regaining BRCA function shows that PARP-targeting drugs act through a synthetic lethal mechanism (*8*). This finding triggered an intensive search for synthetic lethal drug targets akin to PARP. In particular, large-scale RNA interference screens (in which RNA molecules block the expression of specific genes) have led to a growing list of potential synthetic lethal

[1]CeMM Research Center for Molecular Medicine of the Austrian Academy of Sciences, Vienna, Austria. [2]Sage Bionetworks, 1100 Fairview Avenue North, Seattle, WA 98109, USA. E-mail: snijman@cemm.oeaw.ac.at; friend@sagebase.org